

Electronic Supplementary Information

New thiophene-based conjugated macrocycles for optoelectronic applications

John Marques dos Santos,^a Lethy Krishnan Jagadamma,^b Joseph Cameron,^a Alan A. Wiles,^a Claire Wilson,^a Peter J. Skabara,^{a*} Ifor D. W. Samuel,^{b*} Graeme Cooke^{a*}

^a *School of Chemistry, University of Glasgow, Glasgow, G12 8QQ, UK.*

^b *Organic Semiconductor Centre, SUPA, School of Physics and Astronomy, University of St. Andrews, St. Andrews, Fife, KY16 9SS, UK.*

E-mail: Peter.skabara@glasgow.ac.uk; idws@st-andrews.ac.uk; Graeme.Cooke@glasgow.ac.uk.

Keywords: Macrocycle, thiophene, fullerene, solar cell, photodetectors, OFETs, electrochemistry.

1. Prior examples of conjugated macrocycles applied in OPV devices

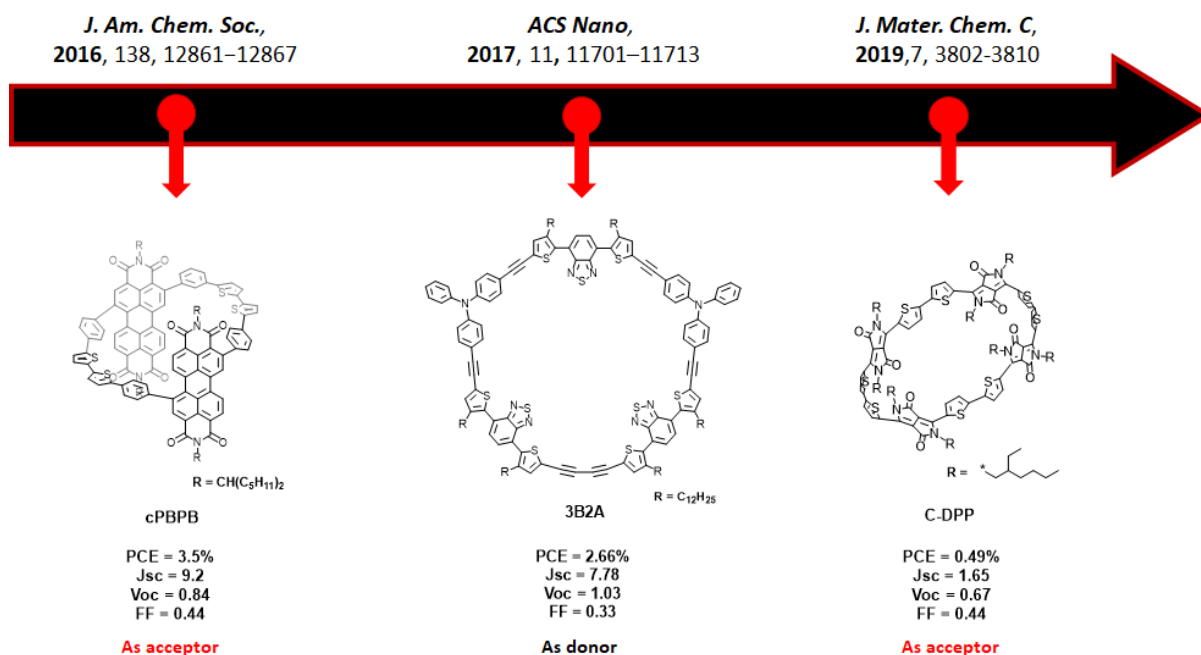


Figure S1. Prior literature examples of purely organic conjugated macrocycles applied in OPV devices.

2. Materials

All the reagents were purchased from either Sigma Aldrich[®], Fluorochem[®], TCI[®], Alfa Aesar[®], Acros[®] or Fisher Scientific[®] and used as received. Column chromatography was carried out using silica gel (Sigma-Aldrich) 40 – 63 nm 60 Å. The solvent system is specified in each experiment. TLCs were performed using Merck silica gel 60 covered aluminium plates F254. Dry solvents were obtained from Innovative Technology inc. Pure Solv 400-5-MD solvent purification system (activated alumina columns) or Sigma Aldrich[®].

3. Methods

3.1. Chemical structure confirmation:

NMRs were recorded on a Bruker Avance III 400 spectrometers. The ^1H and ^{13}C spectra were recorded at 400 and 101 MHz, respectively. Chemical shifts were reported in ppm and coupling constants in Hz as absolute values. Mass spectrometry was obtained from the mass spectrometry service at the University of Glasgow or from National Mass Spectrometry Facility at Swansea University. Melting points (MP) were recorded on a SMP-10 Stuart Scientific melting point machine. Melting points are uncorrected.

3.2. Optical absorbance and photoluminescence measurements:

Absorbance spectrometry was performed using a Perkin Elmer Lambda 25 UV/VIS Spectrometer at room temperature, while the solution photoluminescence (PL) measurements were performed using a Shimadzu RF-5301PC spectro-fluorimeter. Solutions were measured in dilute dichloromethane solution (5×10^{-6} M).

3.3. Electrochemical measurements:

Electrochemistry was performed using a CH Instrument Electrochemical Workstation (CHI 440a), Austin, TX, USA. Samples were analysed at 1×10^{-3} M concentrations (in dichloromethane) with a scan rate of 0.07 V/s using TBA[PF]₆ (0.1 M in corresponding solvent) as the supporting electrolyte. A platinum disk working electrode, a platinum wire counter electrode and a silver wire quasi-reference were used for all measurements. The reduction potentials are referred to ferrocene (external reference) with the Fc/Fc⁺ redox couple adjusted to 0.00 V. Ionisation energies (IE), electron affinities (EA) and the HOMO-LUMO energy gap (E_{fund}) were calculated using:

$$IE = -[E_{ox} + 4.8] \text{ eV} \quad (1)$$

$$EA = -[E_{red} + 4.8] \text{ eV} \quad (2)$$

$$E_{fund} = |IE - EA| \text{ eV} \quad (3)$$

All the spectroscopic and electrochemical data were processed using Origin Pro 8.5 software suite.

3.4. Theoretical calculations:

DFT calculations were undertaken using the Gaussian 09 software suite.¹ Molecular geometries were initially optimised semi-empirically (PM6) and then re-optimised by DFT [B3LYP/6-311G(d,p) level]. The hexyl chains were replaced by methyl units to facilitate the convergence of the geometry optimisations.

3.5. Organic field-effect transistors

Prefabricated substrates were purchased from Fraunhofer IPMS. These substrates were n-doped silicon (gate electrode) with 230 nm SiO₂ dielectric and 30 nm Au patterned source-drain electrodes. Measurements were carried out on transistors with 1 cm channel width and channel lengths of 5 μm, 10 μm and 20 μm.

For fabrication of bottom-gate bottom-contact OFETs, the substrates were washed using deionized H₂O, acetone and isopropanol before being dried over a stream of compressed air. The self-assembled monolayer octadecyltrichlorosilane (ODTS) was deposited by preparing a 13 mM solution of ODTS in toluene which was dropcast onto the substrate and left for 5 minutes before washing with toluene, before drying with compressed air. The substrates were then transferred to a nitrogen-filled glovebox (mBraun) and **McT-1** was deposited by spin-coating a 10 mg ml⁻¹ chloroform or toluene solution at 1000 rpm for 60 seconds.

Current-voltage characteristics were carried out using a Keithley 4200 semiconductor characterization system. All measurements were carried out in a nitrogen-filled glovebox and data are reported from an average of 10 devices. Field-effect mobilities were calculated in the saturation regime using the following equation:

$$\mu_{sat} = \frac{2L}{WC_i} \times \left(\frac{\partial \sqrt{I_{ds}}}{\partial V_g} \right)^2$$

3.6. Atomic force microscopy

Atomic force microscopy measurements were carried out in tapping mode using a Bruker Innova instrument. Data was processed using Bruker NanoScope Analysis 1.5 program. The scans consisted of 512 points in 512 lines at a scan rate of 1.0 Hz. Scans were carried out for areas of $5 \times 5 \mu\text{m}^2$, $10 \times 10 \mu\text{m}^2$ and $20 \times 20 \mu\text{m}^2$. Default bow remove process in the NanoScope Analysis program was used to flatten the images.

3.7. Solar cell fabrication and testing

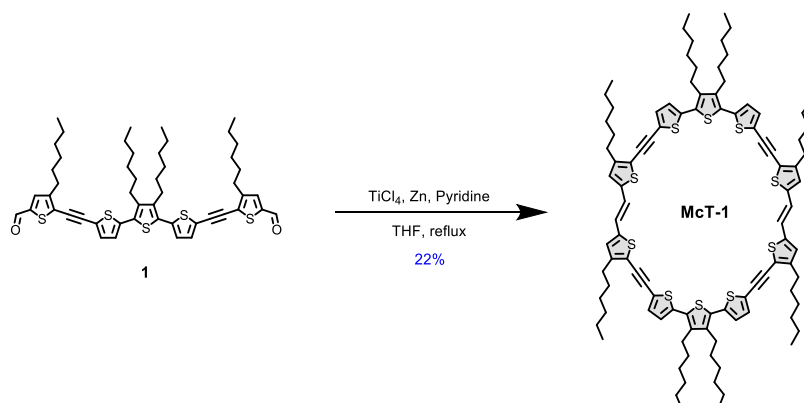
Organic solar cells were fabricated on pre-patterned ITO-coated glass (2 cm x 2 cm). The ITO-coated glass substrates were cleaned in detergent (sodium dodecyl sulphate), successively ultrasonicated in deionized water, acetone, and isopropyl alcohol, and exposed to oxygen in a plasma asher for 3 minutes. For each donor molecule, the photovoltaic performance optimisation process was started with identifying the donor to acceptor ratio (wt%, varying from 1 : 1 to 1 : 4) giving the best photovoltaic performance. The acceptor molecule used was **PC₇₁BM** (American Dye Sources, ADS71BFA) and the total concentration of the D:A blend mixture was 10 mg mL^{-1} in chlorobenzene. Donor and acceptor solutions were stirred separately at $60 \text{ }^\circ\text{C}$ for ~ 3 hours and then the blended mixture was stirred at $60 \text{ }^\circ\text{C}$ for another 4 hours. Devices were made by depositing PEDOT:PSS as hole extraction layer having thickness $\sim 30\text{--}40 \text{ nm}$. The active layer was deposited by spin - coating (900 rpm, 60 s) on glass/ITO/PEDOT:PSS substrates inside a nitrogen filled glove box. The samples were then transferred to a vacuum thermal evaporator (1×10^{-6} mbar base pressure) and kept under vacuum before thermally evaporating the metal contacts consisting of Ca (4nm) and Al (100 nm) using a shadow mask. The active area of the device was 0.08 cm^2 . All the processing related to the active layer was performed inside the nitrogen glove box.

After the electrode deposition, the devices were encapsulated with a UV optical adhesive and a glass coverslip. The current–voltage characteristics were determined under an illumination intensity of 100 mW cm^{-2} in air using an air mass 1.5 global (AM 1.5G) ScienceTech solar simulator (SS150 Class AAA) and a Keithley 2400 source-measure unit. The illumination intensity was verified with a calibrated monosilicon detector with a KG-5 filter. The external quantum efficiency (EQE) measurements were performed at zero bias by

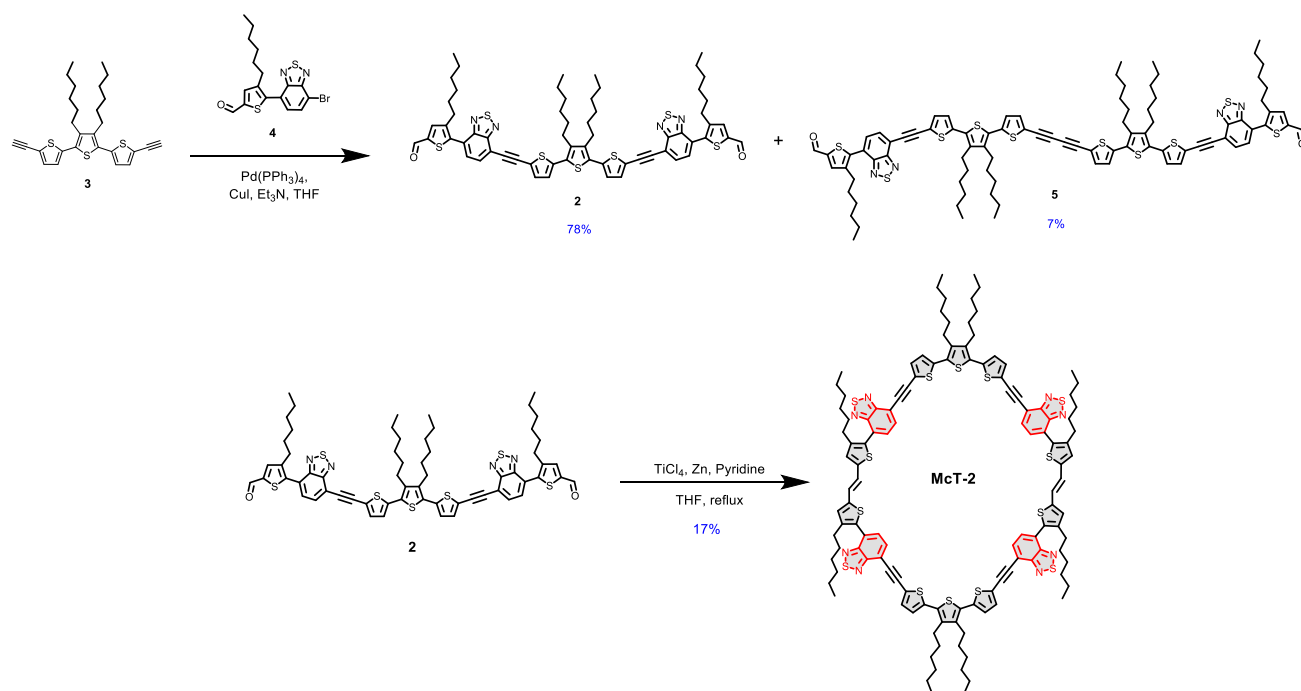
illuminating the device with monochromatic light supplied from a Xenon arc lamp in combination with a dual-grating monochromator.

4. Synthesis

The synthetic pathway towards the target molecules was planned using the typical Sonogashira cross-coupling reaction and the McMurry reaction (**Scheme S1** and **S2**). Compounds **1**, **3** and **4** were obtained following procedures from the literature.^{2,3} Then, compound **2** was synthesized via Sonogashira coupling and **5** was obtained as side product via competing Glaser side-reaction (**Scheme S2**).



Scheme S1. Synthesis of **McT-1**.



Scheme S2. Synthetic pathway towards **McT-2**.

Tables **S1** and **S2** show different concentrations of compounds **1** and **2** used in the synthesis of **McT-1** and **McT-2**, respectively. The yield improved significantly by going from 1.8 mM (2%) to 3.6 mM (22%) in the case of **McT-1**, and from 7% to 17% on going from 1.0 mM to 1.3 mM in the case of **McT-2**. Further increasing the concentration of the reaction decreased the yield in both cases possibly due to competing polymerization. The reaction total time was 8 hours, and increasing it to 24 hours or 48 hours did not result in yield improvement.

Table S1. Conditions used to synthesize compound **McT-1**.

Condition	Final concentration of comp. 1	Solvent	R. total time	Yield
1	1.8 mM	THF	8 h	2%
2	2.6 mM	THF	8 h	12%
3	3.6 mM	THF	8 h	22%
4	5.0 Mm	THF	8 h	9%

Table S2. Conditions used to synthesize compound **Mct-2**.

Condition	Final concentration of comp. 2	Solvent	R. total time	Yield
1	1.0 mM	THF	8 h	7%
2	1.3 mM	THF	8 h	17%
3	2.0 mM	THF	8 h	10%
4	4.0 mM	THF	8 h	5%

Synthesis of Compounds 2 and 5:

Compounds **3** (200 mg, 0.43 mmol), **4** (386 mg, 0.94 mmol) and dry triethylamine (10 mL) were dissolved in dry tetrahydrofuran (10 mL) under an argon atmosphere. Subsequently, copper (I) iodide (8.0 mg, 0.04 mmol) and tetrakis(triphenylphosphine)palladium(0) (50.0 mg, 0.04 mmol) were added to the mixture and the solution was stirred at 50 °C overnight. The mixture was then diluted with dichloromethane (50 mL) and washed with brine (3 × 50 mL). The organic extract was dried over MgSO₄, filtered, and the solvent was removed under reduced pressure. The crude product was purified by flash column chromatography over silica gel (petroleum ether 40 - 60 °C :dichloromethane; 1:9) to yield compounds **2** as a purple solid (369 mg, 78%) and compound **5** as a purple solid (23 mg, 7 %).

Compound 2: Mp: 107–109 °C; ¹H NMR (400 MHz, CDCl₃) δ 9.94 (s, 2H), 7.87 (d, *J* = 7.3 Hz, 2H), 7.65 (d, *J* = 7.3 Hz, 2H), 7.42 (d, *J* = 3.8 Hz, 2H), 7.12 (d, *J* = 3.8 Hz, 2H), 2.81–2.71 (m, 4H), 2.70–2.58 (m, 4H), 1.64–1.50 (m, 8H), 1.53–1.40 (m, 4H), 1.368–1.33 (m, 8H), 1.28–1.14 (m, 12H), 0.93 (t, *J* = 6.9 Hz, 6H), 0.82 (t, *J* = 6.9 Hz, 6H); ¹³C NMR (101 MHz, CDCl₃) δ 183.0, 154.5, 153.2, 143.4, 143.2, 142.1, 141.4, 139.2, 137.8, 133.9, 132.0, 130.3, 130.1, 127.2, 126.0, 122.0, 117.5, 90.6, 90.4, 31.6, 90.4, 30.7, 30.4, 29.7, 29.5, 29.1, 28.4, 22.7, 22.6, 14.2, 14.1. *m/z* (MALDI⁺) 1120.3072 [M⁺] (C₆₂H₆₄N₄O₂S₇ requires 1120.3074).

Compound 5: Mp: 112–115 °C; ¹H NMR (400 MHz, CDCl₃) δ 9.95 (s, 2H), 7.87 (d, *J* = 7.3 Hz, 2H), 7.65 (d, *J* = 7.3 Hz, 2H), 7.42 (d, *J* = 3.8 Hz, 2H), 7.31 (d, *J* = 3.9 Hz, 2H), 7.11 (d, *J* = 3.8 Hz, 2H), 7.04 (d, *J* = 3.9 Hz, 2H), 2.81–2.70 (m, 8H), 2.68–2.58 (m, 4H) 1.63–1.54 (m, 12H), 1.41–1.39 (m, 8H), 1.37–1.33 (m, 10H), 1.27–1.18 (m, 18H), 0.92 (t, *J* = 6.9 Hz, 12H), 0.82 (t, *J* = 6.9 Hz, 6H); ¹³C NMR (101 MHz, CDCl₃) δ 182.9, 154.4, 153.1, 143.3, 143.1, 142.0, 141.4, 141.3, 139.3, 139.0, 137.7, 134.9, 133.8, 131.9, 130.2, 129.8, 129.8, 127.0, 125.9, 125.7, 121.9, 121.4, 117.3, 90.5, 90.3, 79.3, 77.5, 53.4, 31.5, 31.4, 30.63, 30.3, 29.6, 29.6, 29.4, 29.4, 29.0,

28.3, 28.3, 22.6, 22.5, 14.2, 14.1, 14.0. m/z 1582.4578 (MALDI⁺) [M^+] ($C_{90}H_{94}N_4O_2S_{10}$ requires 1582.4584).

Synthesis of McT-1:

Titanium tetrachloride (0.6 mL, 5 mmol) was added carefully to a suspension of zinc powder (450 mg, 6.88 mmol) and activated molecular sieves (50 mg, 4 Å) in dry tetrahydrofuran (80 mL) under an argon atmosphere at room temperature. The suspension was stirred under reflux for 3 h. Then a solution of compound **1** (500 mg, 0.587 mmol) and pyridine (0.7 mL, 8 mmol) in tetrahydrofuran (80 mL) was added dropwise to the above gently refluxing suspension over a period of 5 h. After refluxing for 2 h, the reaction mixture was cooled to room temperature. A saturated solution of aqueous potassium carbonate (50 mL) was added carefully over 30 minutes, and then chloroform (50 mL) was added carefully. After stirring for 30 minutes, the mixture was washed with aqueous ammonium chloride (3 × 50 mL) and extracted with chloroform (100 mL). The organic extract was dried over $MgSO_4$, filtered, and the solvent was removed under reduced pressure. The crude product was purified by flash column chromatography over silica gel (petroleum ether 40 - 60 °C :dichloromethane; 4:1), followed by a recrystallisation in a mixture of chloroform and hexane to yield **McT-1** as a red solid (105 mg, 22%). Mp > 300 °C; ¹H NMR (400 MHz, $CDCl_3$) δ 7.15 (d, $J = 3.9$ Hz, 4H), 7.00 (d, $J = 3.9$ Hz, 4H), 6.91 (s, 4H), 6.91 (s, 4H), 2.76–2.62 (m, 16H, C(14, 20)), 1.73–1.52 (m, 24H, C(15, 16, 21)), 1.49–1.28 (m, 40H, C(17, 18, 22, 23, 24)), 0.95–0.87 (m, 24H, C(19, 25)); ¹³C NMR (101 MHz, $CDCl_3$) δ 147.9, 142.6, 140.6, 139.1, 131.3, 130.0, 125.2, 123.5, 122.5, 121.0, 117.5, 90.1, 88.3, 31.6, 31.5, 30.3, 30.1, 29.7, 29.6, 28.9, 28.1, 22.6, 22.6, 14.1, 14.0; m/z (MALDI⁺) 1640.6611 [M^+] ($C_{100}H_{120}S_{10}$ requires 1640.6597).

Synthesis of McT-2:

Titanium tetrachloride (0.3 mL, 2.7 mmol) was added carefully to a suspension of zinc powder (210 mg, 3.22 mmol) and activated molecular sieves (30 mg, 4 Å) in dry tetrahydrofuran (100 mL) under an argon atmosphere at room temperature. The suspension was stirred under reflux for 3 h. Then a solution of compound **2** (300 mg, 0.27 mmol) and pyridine (0.35 mL, 4.34 mmol) in tetrahydrofuran (100 mL) was added dropwise to the above gently refluxing suspension over a period of 5 h. After refluxing for 2 h, the reaction mixture was cooled to room temperature. A saturated solution of potassium carbonate (50 mL) was added carefully during 30 minutes, and then chloroform (50 mL) was added carefully. After stirring for 30 minutes, the mixture was washed with aqueous ammonium chloride (3 × 50 mL) and extracted with chloroform (100 mL). The organic extract was dried over MgSO₄, filtered, and the solvent was removed under reduced pressure. The crude product was purified by flash column chromatography over silica gel (petroleum ether 40 - 60 °C :dichloromethane; 2:3), followed by a recrystallisation in a mixture of toluene and hexane to yield **McT-2** as a dark purple solid (50 mg, 17%). Mp > 300 °C; ¹H NMR (400 MHz, CDCl₃) δ 7.80 (d, *J* = 7.4 Hz, 4H), 7.60 (d, *J* = 7.4 Hz, 4H), 7.35 (d, *J* = 3.8 Hz, 4H), 7.14 (s, 4H), 7.06, (s, 4H), 7.05 (d, *J* = 3.8 Hz, 4H), 2.75–2.67 (m, 16H), 1.71–1.53 (m, 16H), 1.49–1.42 (m, 8H), 1.42–1.33 (m, 16H), 1.33–1.17 (m, 24H), 0.93 (t, *J* = 7.0 Hz, 12H), 0.87 (t, *J* = 6.8 Hz, 12H); ¹³C NMR (101 MHz, CDCl₃) δ 154.8, 153.5, 143.2, 142.9, 141.1, 140.0, 133.2, 133.0, 132.4, 131.7, 130.3, 129.5, 128.6, 126.7, 124.2, 122.2, 121.1, 115.7, 90.9, 89.7, 31.7, 31.7, 30.6, 30.0, 29.8, 29.7, 29.3, 28.3, 22.8, 22.7, 14.2, 14.1; *m/z* (MALDI⁺) 2178.7 [M⁺] (C₁₂₄H₁₂₈N₈S₁₄ requires 2178.6).

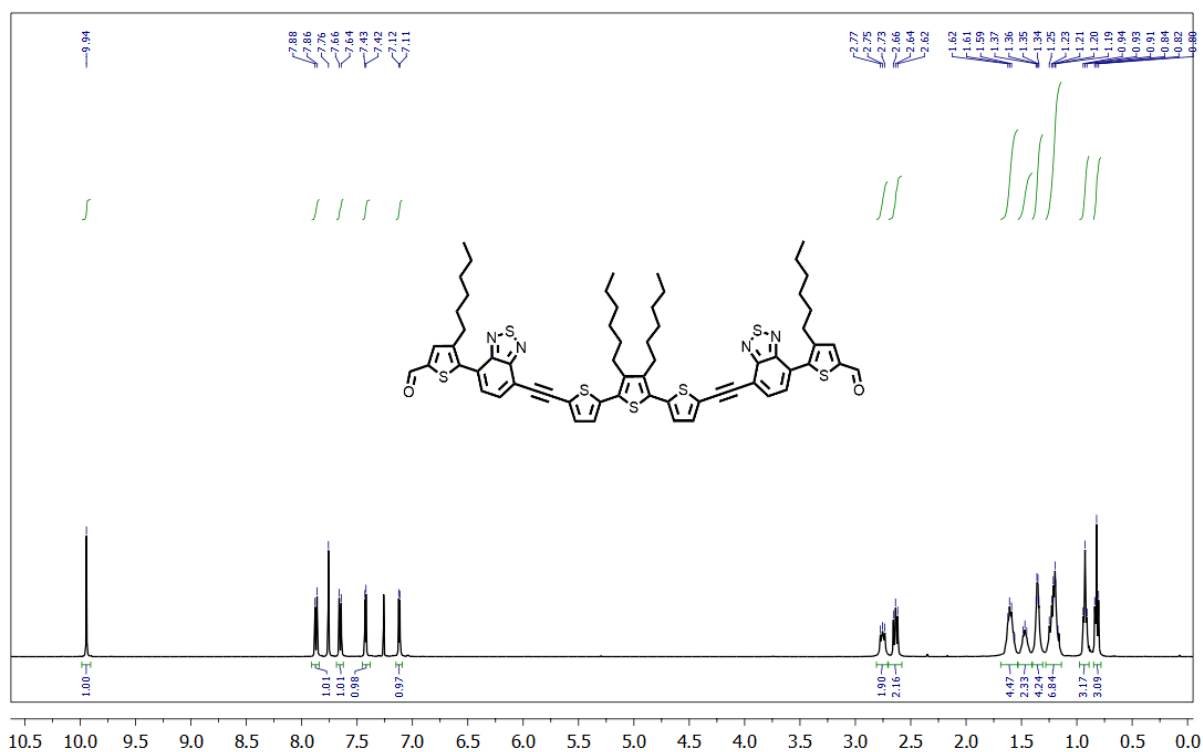


Figure S2: ^1H NMR spectrum (400 MHz, CDCl_3) of compound 2.

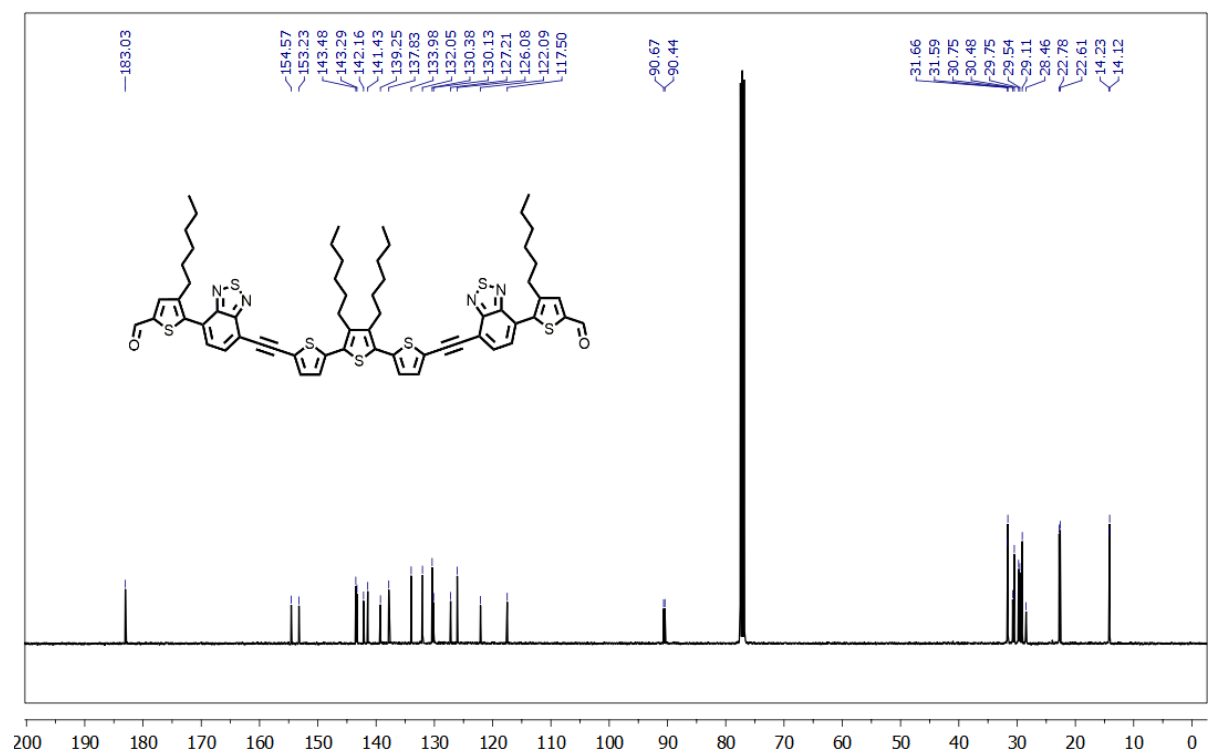


Figure S3: ^{13}C NMR spectrum (101 MHz, CDCl_3) of compound 2.

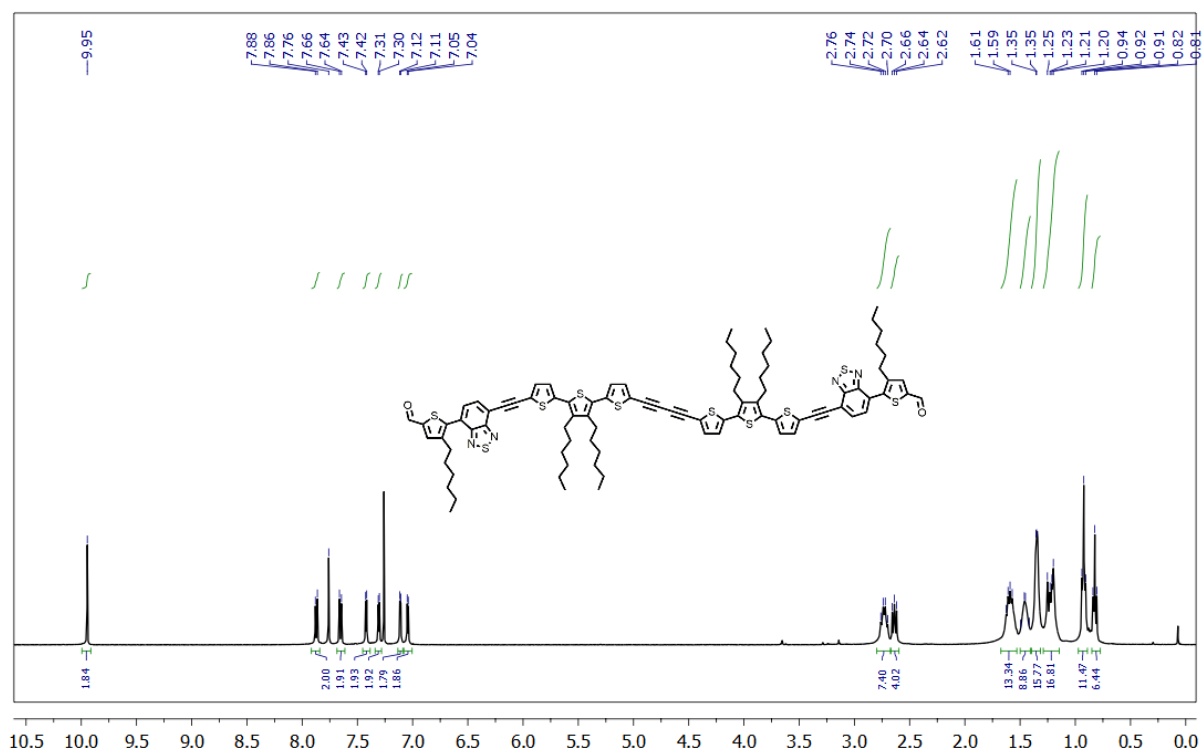


Figure S4: ^1H NMR spectrum (400 MHz, CDCl_3) of compound 5.

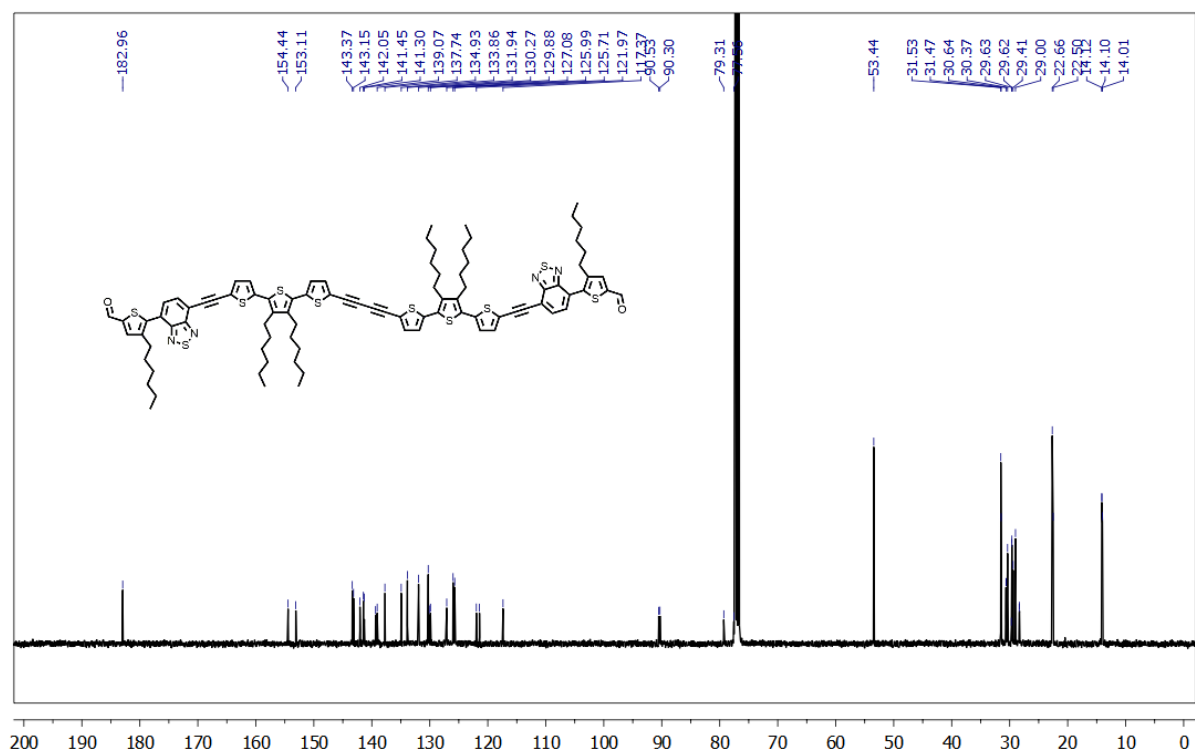


Figure S5: ^{13}C NMR spectrum (101 MHz, CDCl_3) of compound 5.

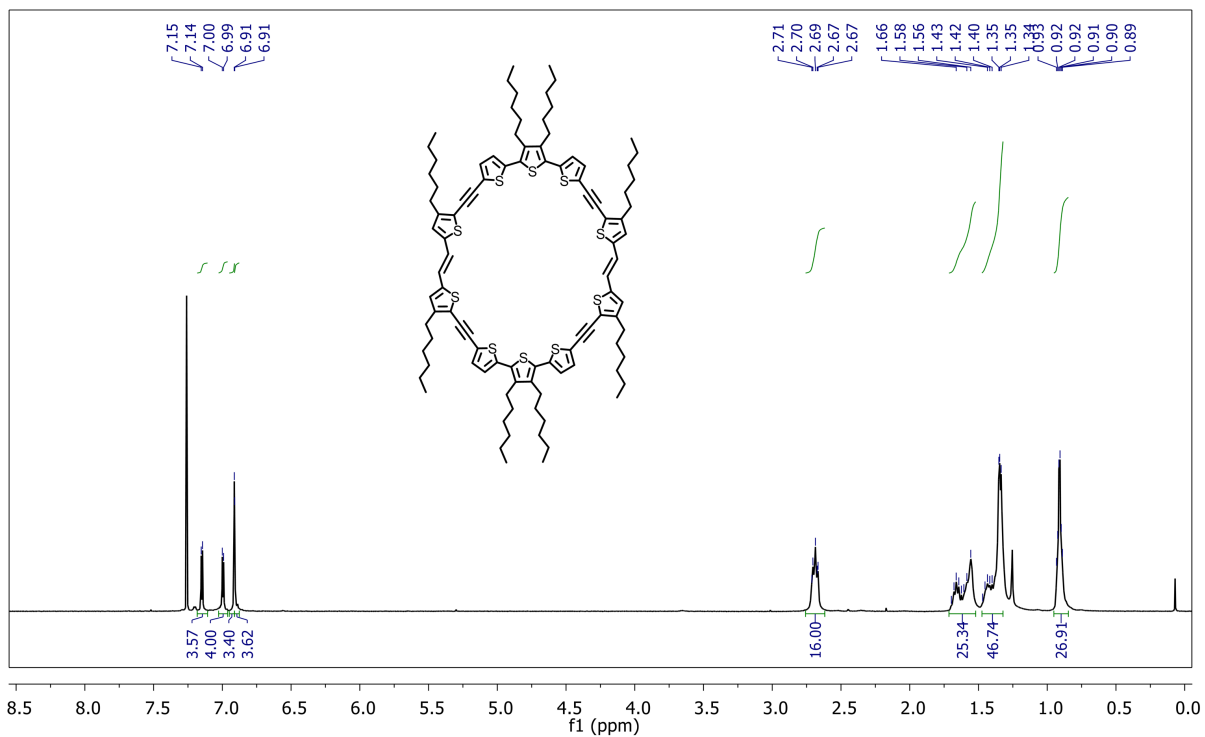


Figure S6: ¹H NMR spectrum (400 MHz, CDCl₃) of McT-1.

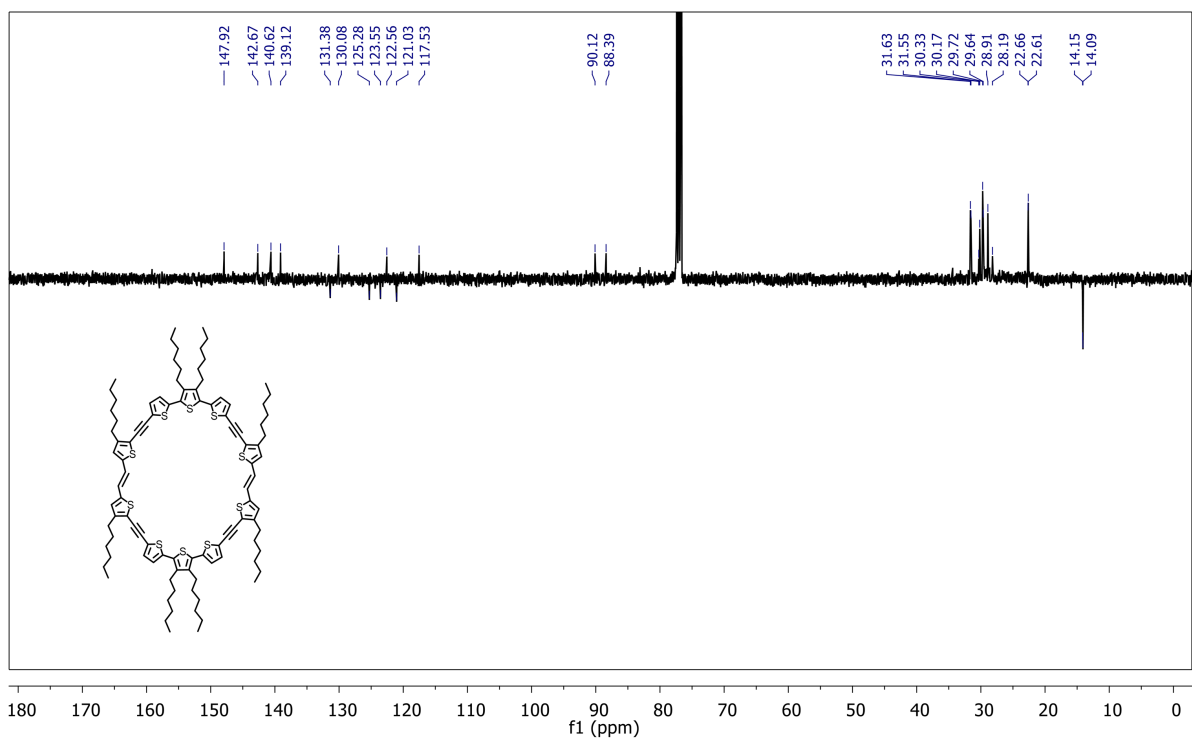


Figure S7: ¹³C NMR spectrum (101 MHz, CDCl₃) of McT-1.

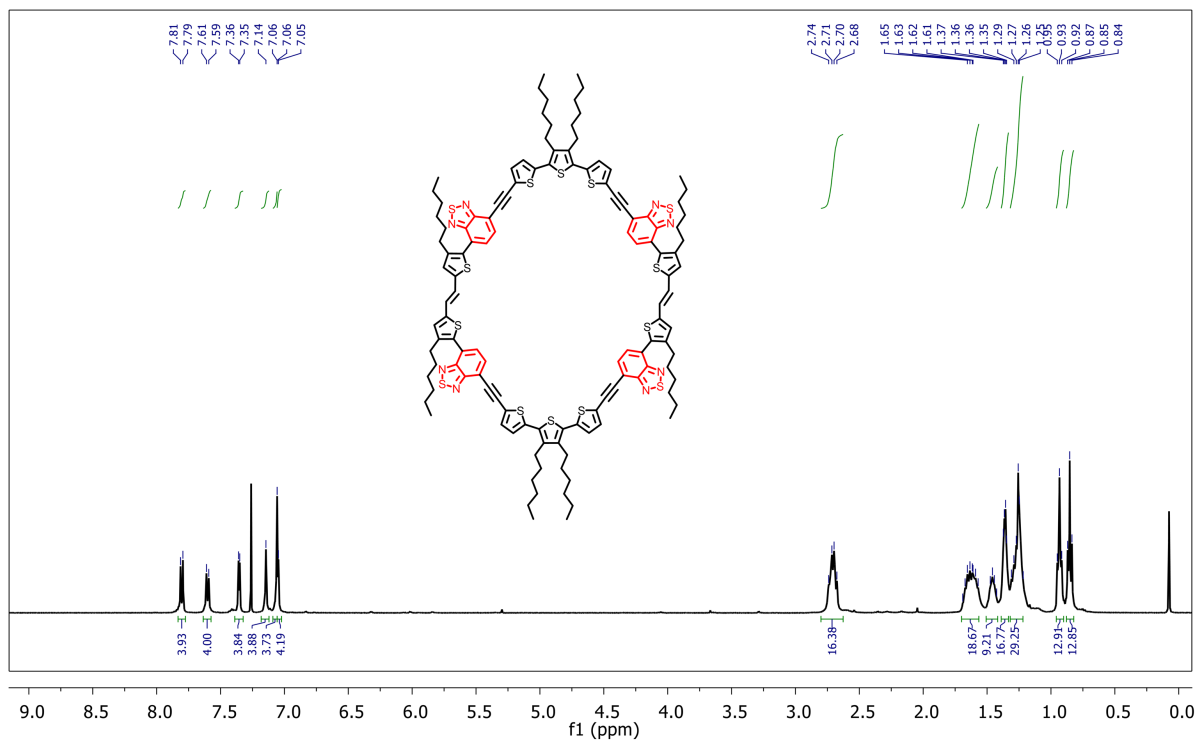


Figure S8: ^1H NMR spectrum (400 MHz, CDCl_3) of Mct-2.

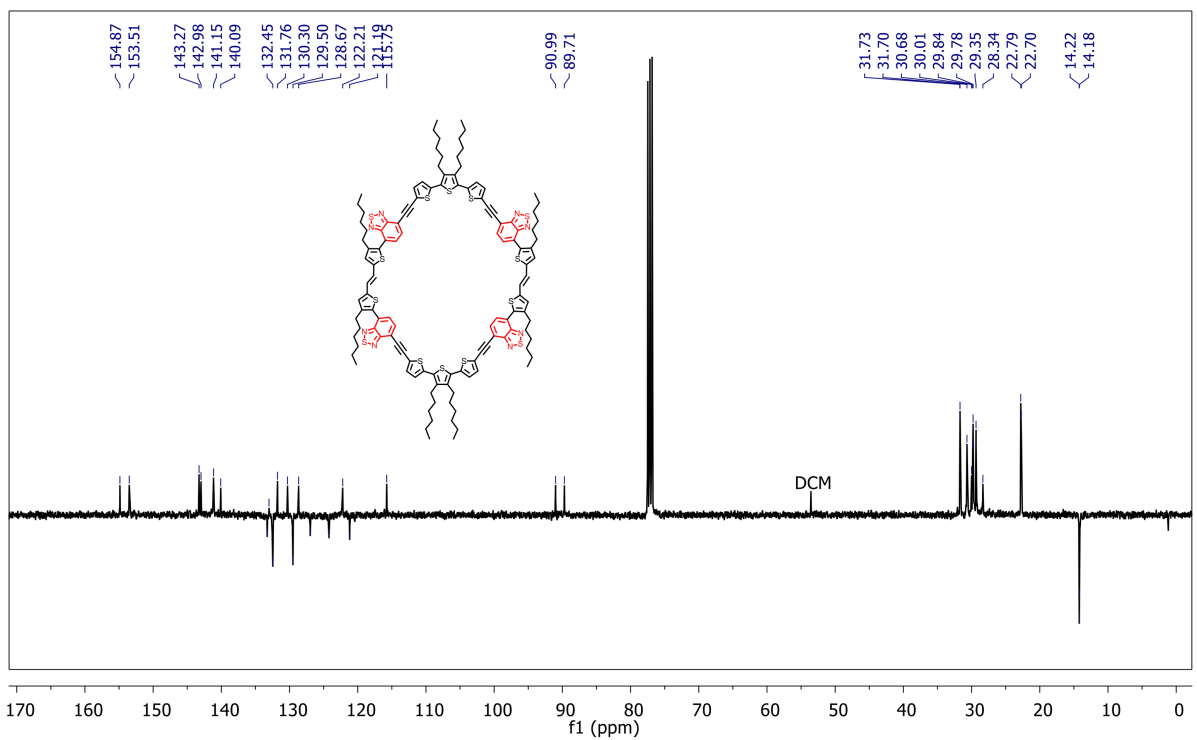


Figure S9: ^{13}C NMR spectrum (101 MHz, CDCl_3) of Mct-2.

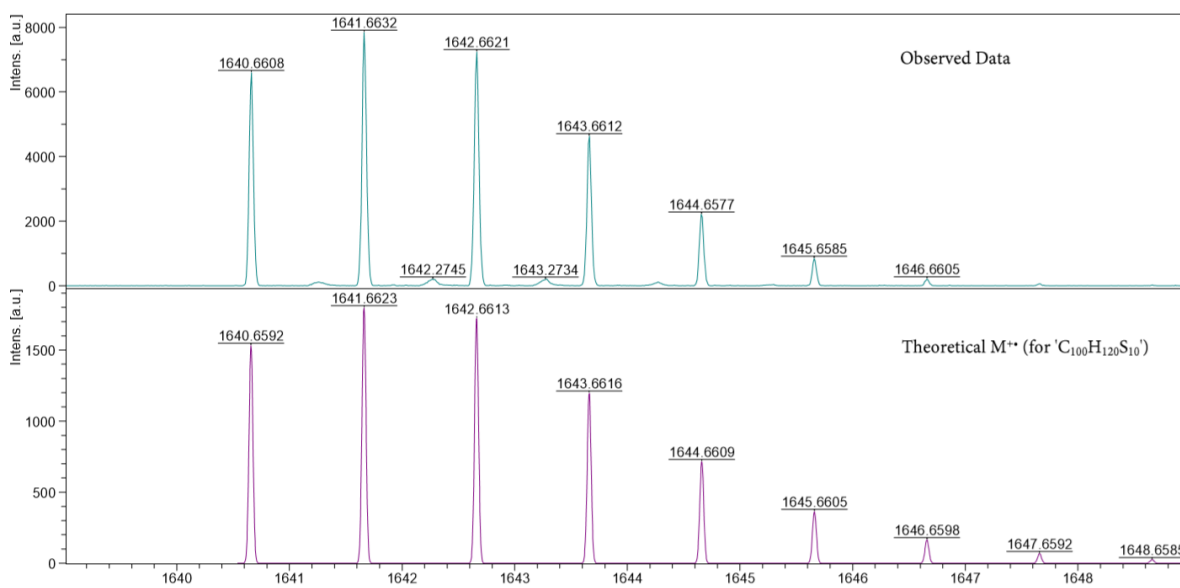


Figure S10: Mass spectrum of **Mct-1** (MALDI, top: experimental, bottom: simulated).

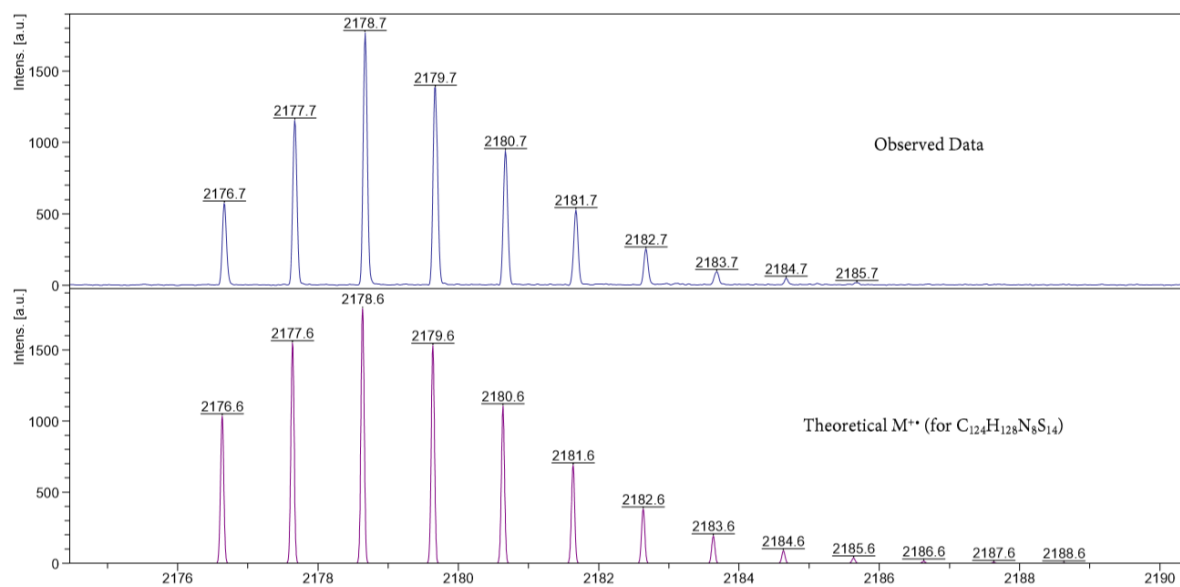


Figure S11: Mass spectrum of **Mct-2** (MALDI, top: experimental, bottom: simulated).

5. Thermogravimetric analysis (TGA) and differential scanning calorimetry (DSC)

Thermogravimetric analysis using a Netzsch TG 209 F3 Tarsus Thermogravimetric Analyser. The experiments were carried out under a flow of nitrogen and from 25°C - 550°C at a heating rate of 10 K min⁻¹. Differential scanning calorimetry was determined on a Netzsch DSC 214 Polyma instrument under nitrogen. Heat-cool-heat cycles were scanned between 25 - 300°C for **McT-1** and between 25-200°C for **McT-2** due to its reduced thermal stability. The heating/cooling rate was 10 K min⁻¹. The first heat cycle was to remove thermal history from the molecule and the subsequent cool and heat scans are presented in **Figure S13**.

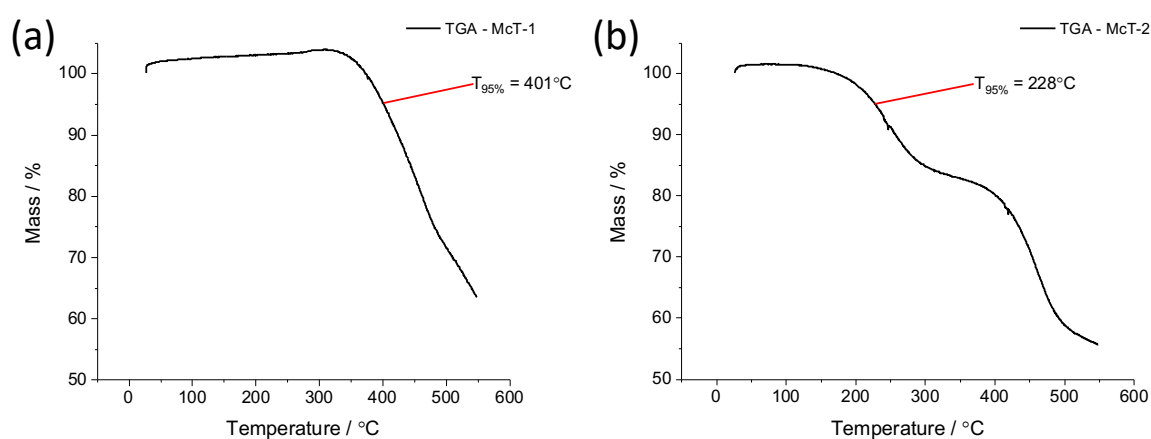


Figure S12. Thermogravimetric analysis of (a) **MCT-1** and (b) **McT-2**

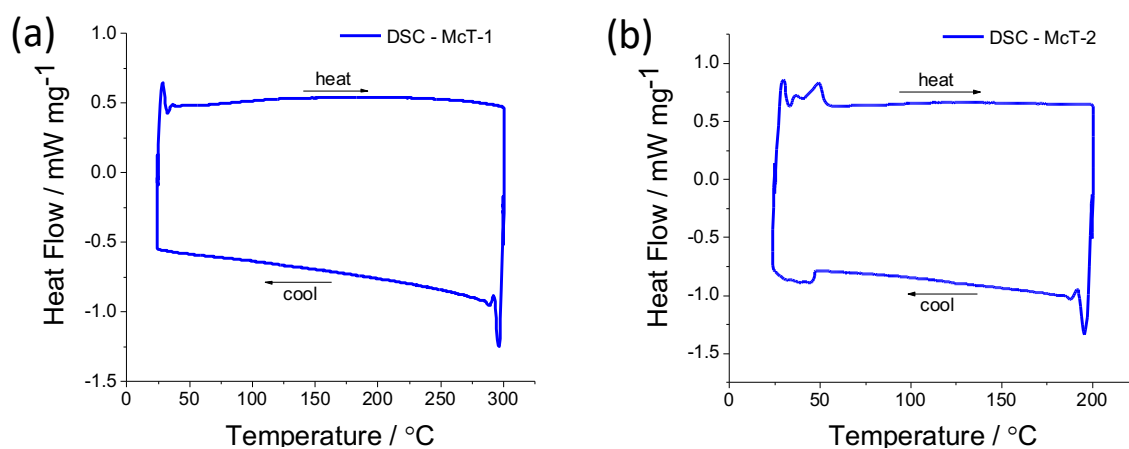


Figure S13. Differential scanning calorimetry of (a) **MCT-1** and (b) **McT-2**

6. UV-vis and fluorescence studies

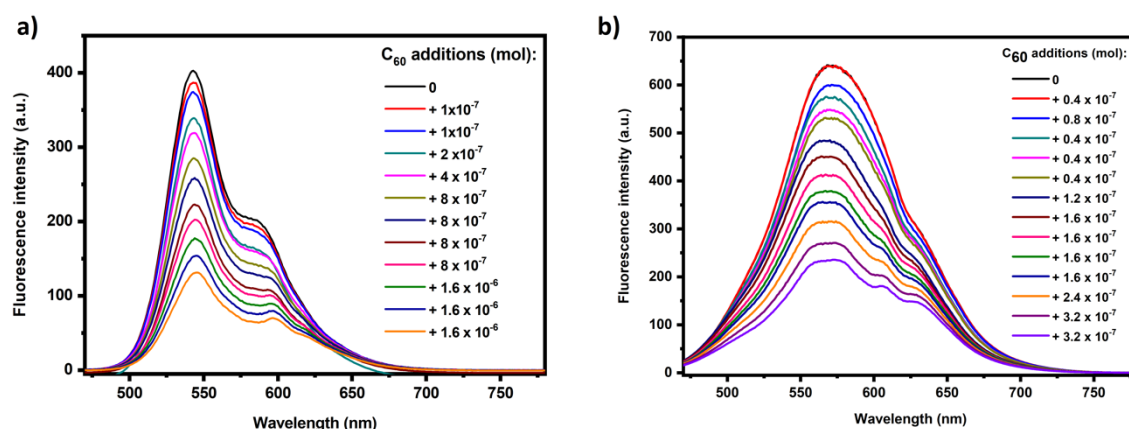


Figure S14. Fluorescence titration of **McT-1** ((a), 1x10⁻⁵ M starting concentration in toluene solution) and **McT-2** ((b), 5x10⁻⁶ M starting concentration in toluene solution) with C₆₀. Each line represents the fluorescence intensity upon each addition of C₆₀ in mol [additions were made in dilute solution (i.e. 1x10⁻³ M) in toluene].

7. Electrochemistry

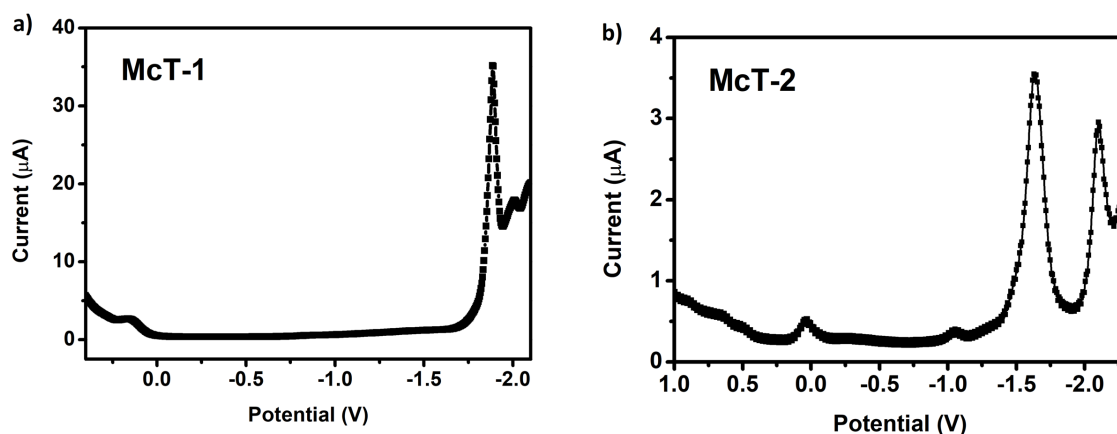


Figure S15. Square wave voltammograms of **McT-1** (a) and **McT-2** (b), recorded in CH₂Cl₂ solution (1x10⁻³ M). The electrodes used were a 1.6 mm diameter platinum working electrode, a platinum wire counter electrode and a silver wire quasi-reference electrode and the electrolyte of choice was TBA.PF₆ (0.1 M). Voltammograms were calibrated versus the ferrocene/ferrocenium (Fc/Fc⁺) redox couple as an external standard.

8. DFT studies

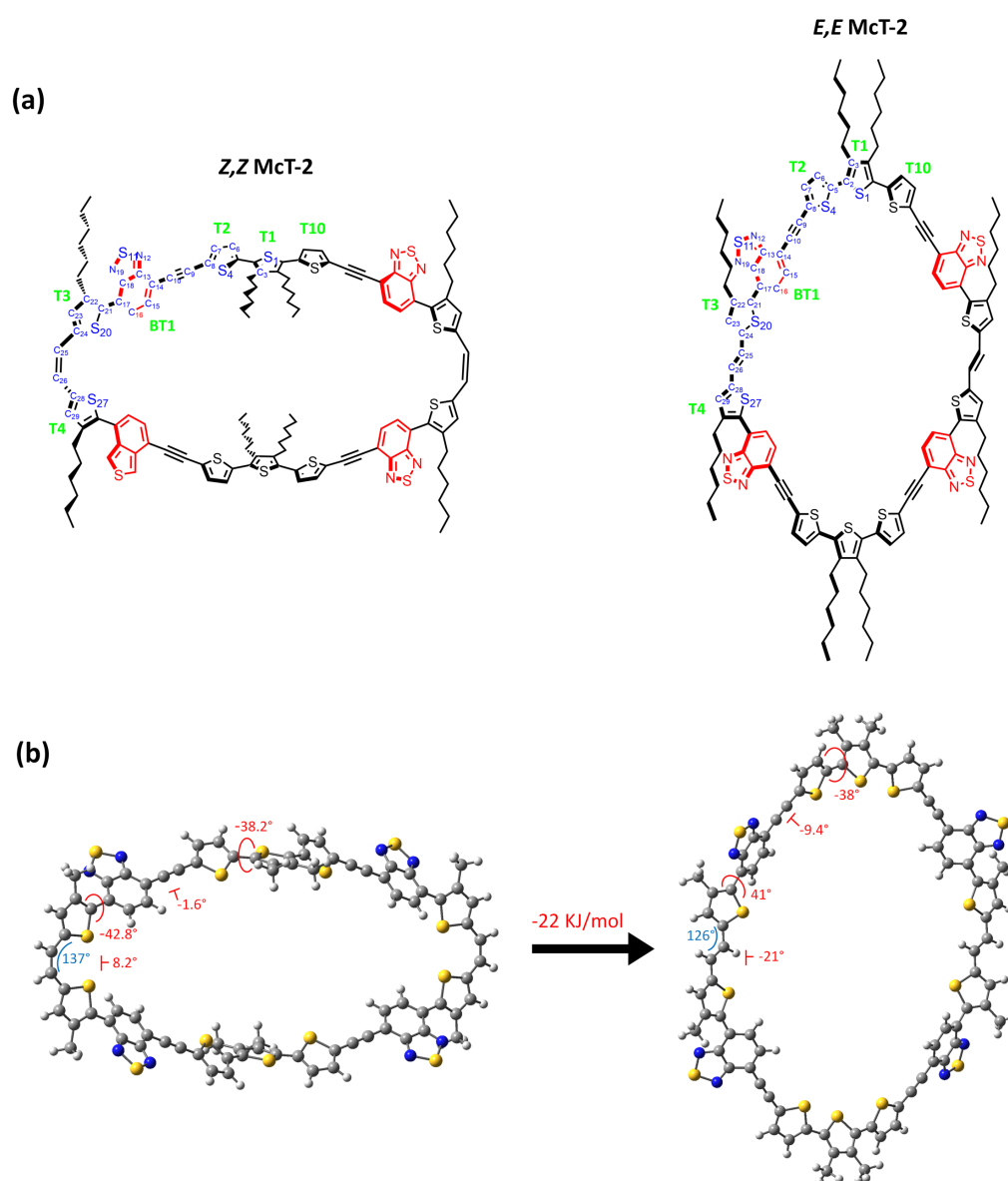


Figure S16. (a) Molecular structure of *Z,Z* and *E,E* isomers of **McT-2** (some atom are labeled, and T1-10 represents thiophene moieties). (b) Optimised structure from DFT (B3LYP/6-311G(d,p)) of *Z,Z* **McT-1** and *E,E* **McT-2**, the difference in energy (KJ) between the isomers is also represented.

Table S3. Computed energy levels of **McT-1** and **McT-2** (DFT; B3LYP/6311G d,p) compared with their voltammetry data.

Dye	HOMO (eV) ^a	LUMO (eV) ^a	ΔE or E_{gap} (eV) ^a	IE (eV) ^b	EA (eV) ^b	E_{fund} (eV) ^b
McT-1	-4.83	-2.57	2.27	-5.0	-2.9	2.1
McT-2	-5.09	-3.01	2.09	-4.8	-3.2	1.6

^a Obtained *via* DFT calculation (5×10^{-6} M); ^b Obtained experimentally *via* electrochemical measurements.

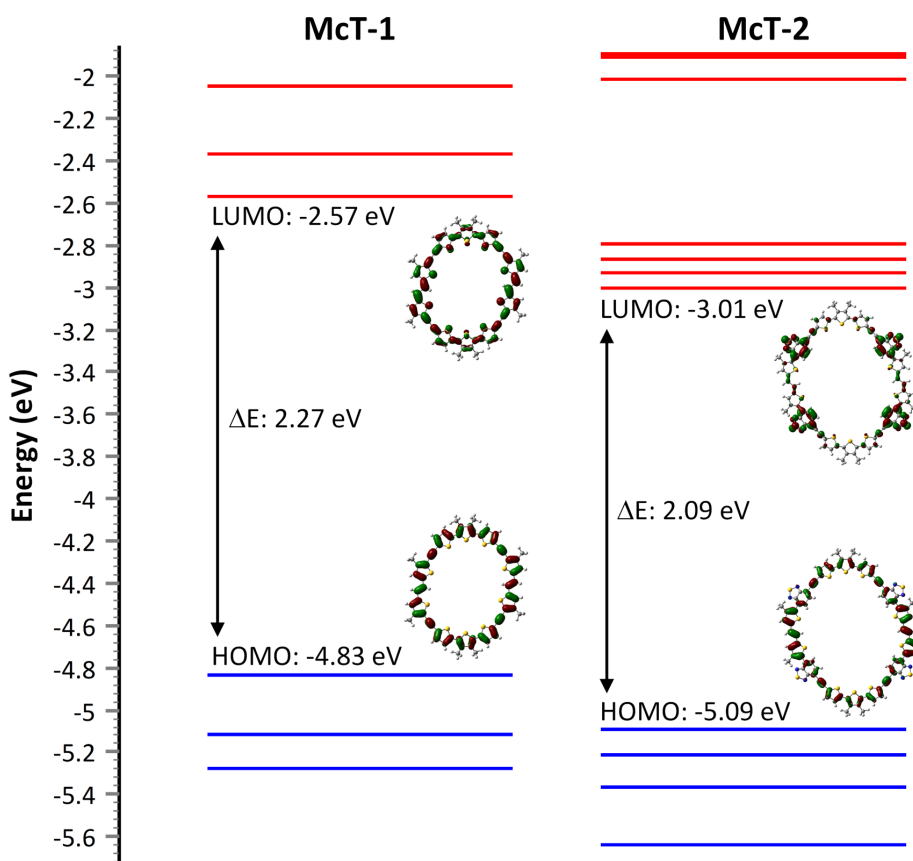


Figure S17. Molecular orbital energies of **McT-1** (left) and **McT-2** (right) obtained from DFT calculations (B3LYP/6-311G d,p in the gas-phase).

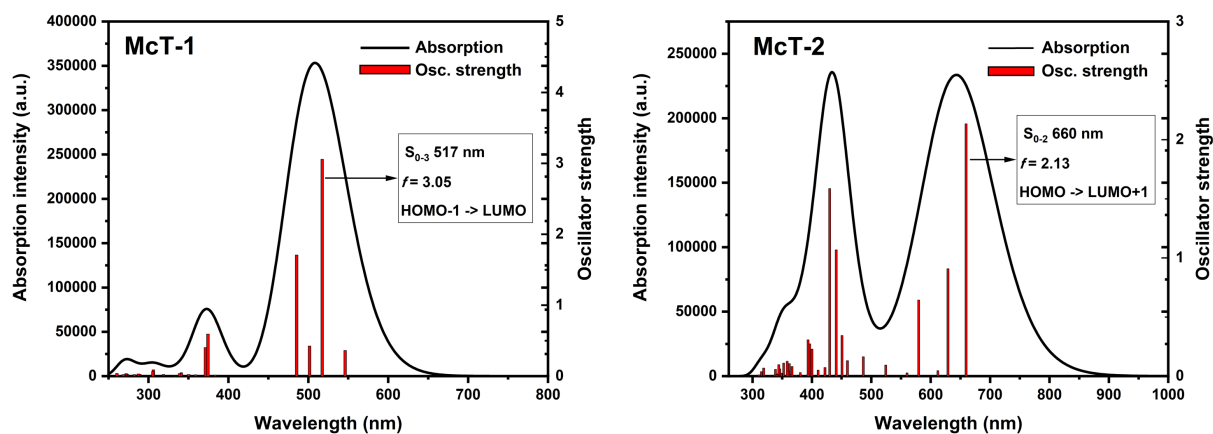


Figure S18. Time dependent DFT simulated (B3LYP/6-311G d,p in the gas-phase) UV-vis spectra of **McT-1** (left) and **McT-2** (right). The oscillator strength for each simulated transition (in red) is also shown.

Table S4. Excitation energies (nm), of predicted absorbance maxima, electronic transition configurations and oscillator strengths (B3LYP/6-311G d,p level) of **MCT-1**.

MCT-1				
State	Symbol	Wavelength (nm)	Oscillator Strength (f)	Transitions (probability)
1	S ₁	663.23	0.0000	HOMO → LUMO (93%) HOMO-2 → LUMO+2 (3%) HOMO-1 → LUMO+1 (3%)
2	S ₂	546.11	0.3628	HOMO → LUMO+1 (81%) HOMO-1 → LUMO (19%)
3	S ₃	517.31	3.0574	HOMO-1 → LUMO (80%) HOMO → LUMO+1 (19%)
4	S ₄	501.53	0.4239	HOMO-2 → LUMO (90%) HOMO → LUMO+2 (8%)
5	S ₅	496.31	0.0000	HOMO-1 → LUMO+1 (87%) HOMO → LUMO (5%) HOMO-2 → LUMO+2 (6%)
6	S ₆	485.32	1.7078	HOMO → LUMO+2 (90%) HOMO-2 → LUMO (8%)
15	S ₁₅	381.43	0.0000	HOMO-4 → LUMO (56%) HOMO-2 → LUMO+2 (6%) HOMO-3 → LUMO (5%) HOMO-1 → LUMO+1 (3%) HOMO → LUMO+4 (10%) HOMO → LUMO+3 (17%)
16	S ₁₆	374.35	0.5933	HOMO-1 → LUMO+4 (43%) HOMO-3 → LUMO+1 (19%) HOMO-4 → LUMO+1 (5%) HOMO-1 → LUMO+3 (6%) HOMO-2 → LUMO+3 (21%)
17	S ₁₇	371.28	0.4032	HOMO-4 → LUMO+1 (50%) HOMO-1 → LUMO+3 (17%) HOMO-2 → LUMO+4 (12%) HOMO-1 → LUMO+4 (7%) HOMO → LUMO+5 (6%) HOMO-3 → LUMO+2 (3%) HOMO-2 → LUMO+3 (4%)
18	S ₁₈	358.81	0.0201	HOMO → LUMO+5 (36%) HOMO-3 → LUMO+2 (25%) HOMO-2 → LUMO+4 (18%) HOMO-1 → LUMO+4 (2%) HOMO-6 → LUMO (5%) HOMO-1 → LUMO+3 (6%)
19	S ₁₉	355.65	0.0013	HOMO-2 → LUMO+3 (65%) HOMO-1 → LUMO+4 (18%) HOMO-4 → LUMO+2 (6%) HOMO-5 → LUMO (5%)
20	S ₂₀	350.30	0.0237	HOMO-2 → LUMO+4 (54%) HOMO-1 → LUMO+3 (7%) HOMO → LUMO+5 (38%)

Table S5. Excitation energies (nm), of predicted absorbance maxima, electronic transition configurations and oscillator strengths (B3LYP/6-311G d,p level) of **MCT-2**.

MCT-2				
State	Symbol	Wavelength (nm)	Oscillator Strength (<i>f</i>)	Transitions (probability)
1	S ₁	722.10	0.0000	HOMO → LUMO (77%) HOMO-1 → LUMO+1 (16%) HOMO-2 → LUMO+2 (5%)
2	S ₂	659.49	2.1341	HOMO → LUMO+1 (63%) HOMO-1 → LUMO (34%)
3	S ₃	629.04	0.9082	HOMO → LUMO+2 (84%) HOMO-2 → LUMO (3%) HOMO-1 → LUMO+3 (11%)
4	S ₄	612.06	0.0471	HOMO-1 → LUMO (63%) HOMO → LUMO+1 (35%)
5	S ₅	607.83	0.0000	HOMO → LUMO+3 (65%) HOMO-1 → LUMO+2 (32%)
6	S ₆	598.52	0.0000	HOMO-1 → LUMO+1 (78%) HOMO → LUMO (19%)
19	S ₁₉	450.77	0.0000	HOMO → LUMO+4 (69%) HOMO-1 → LUMO+6 (9%) HOMO-2 → LUMO+5 (9%) HOMO-4 → LUMO+3 (2%) HOMO → LUMO+7 (5%)
20	S ₂₀	450.64	0.3442	HOMO-4 → LUMO+2 (89%) HOMO-5 → LUMO (4%)
21	S ₂₁	440.91	1.0683	HOMO → LUMO+5 (88%) HOMO-2 → LUMO+4 (9%)
22	S ₂₂	440.63	0.0000	HOMO-4 → LUMO+3 (88%) HOMO → LUMO+4 (5%) HOMO-5 → LUMO+1 (3%)
23	S ₂₃	429.96	1.5863	HOMO → LUMO+6 (47%) HOMO-1 → LUMO+4 (25%) HOMO-4 → LUMO+2 (3%) HOMO-1 → LUMO+7 (7%) HOMO-5 → LUMO (14%)
24	S ₂₄	422.03	0.0726	HOMO-5 → LUMO (68%) HOMO-1 → LUMO+4 (21%) HOMO-4 → LUMO+2 (3%) HOMO → LUMO+6 (3%)

Figure S19. Selected molecular orbital density maps of **McT-1** (B3LYP/6311G d,p).

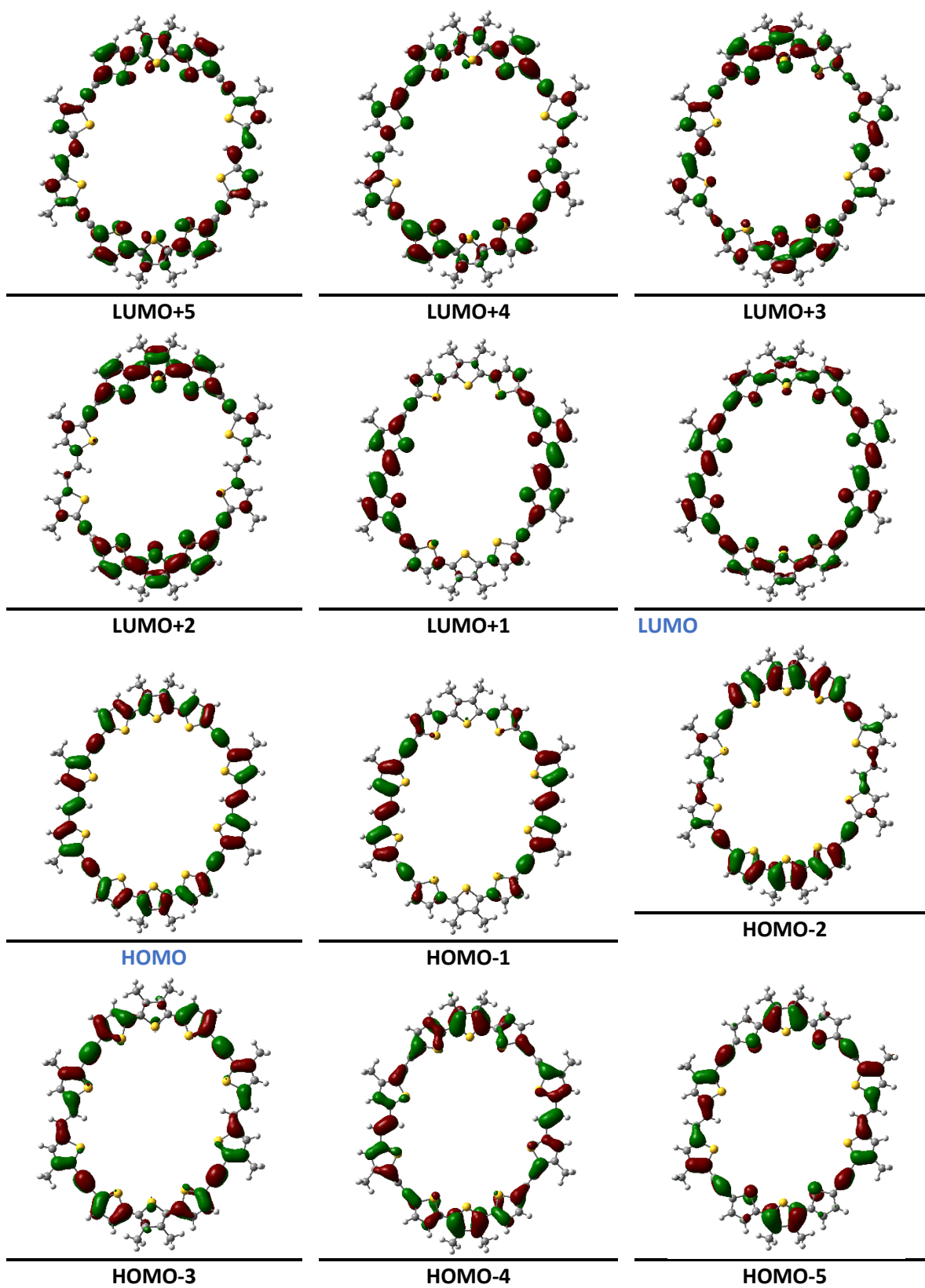
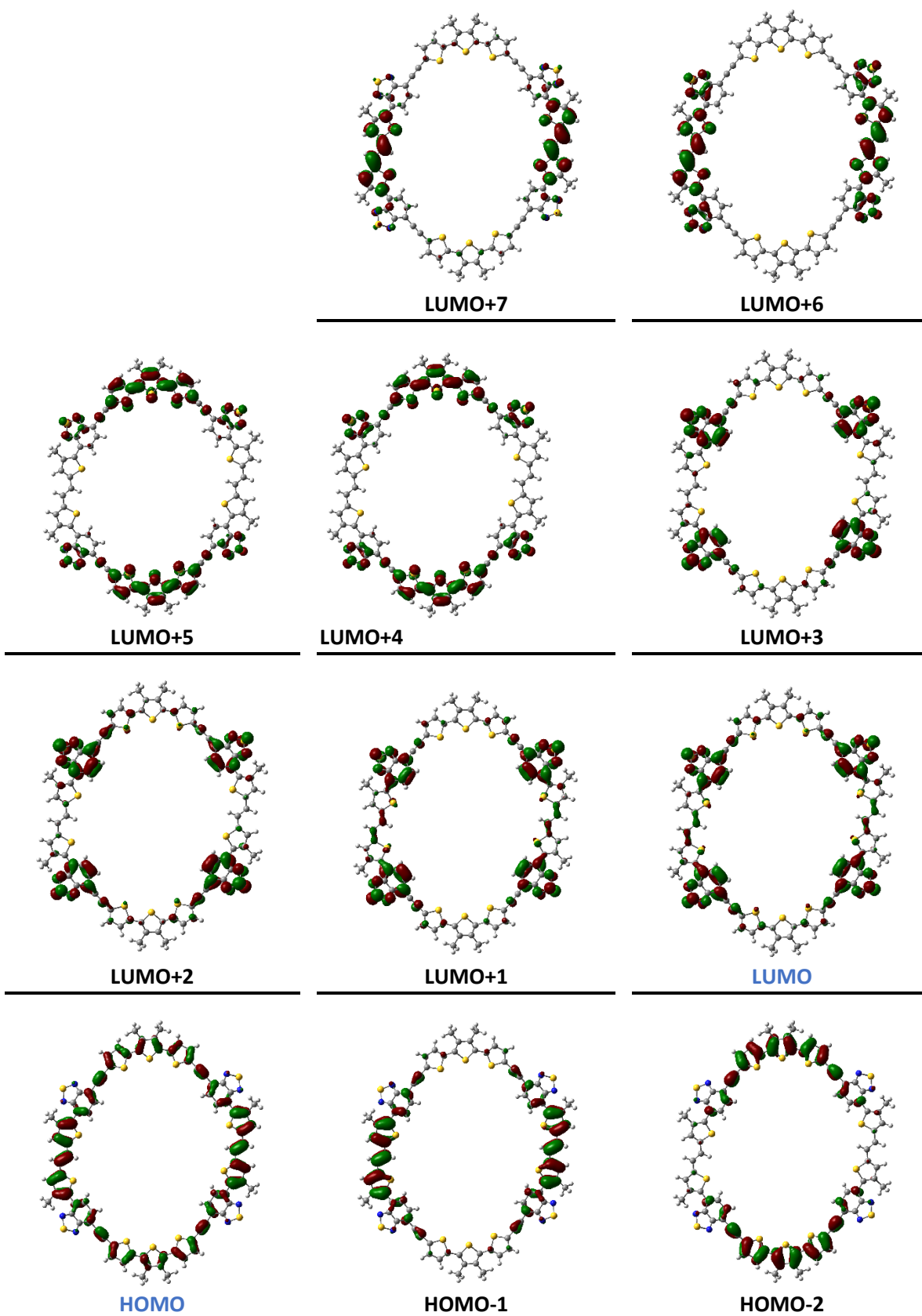


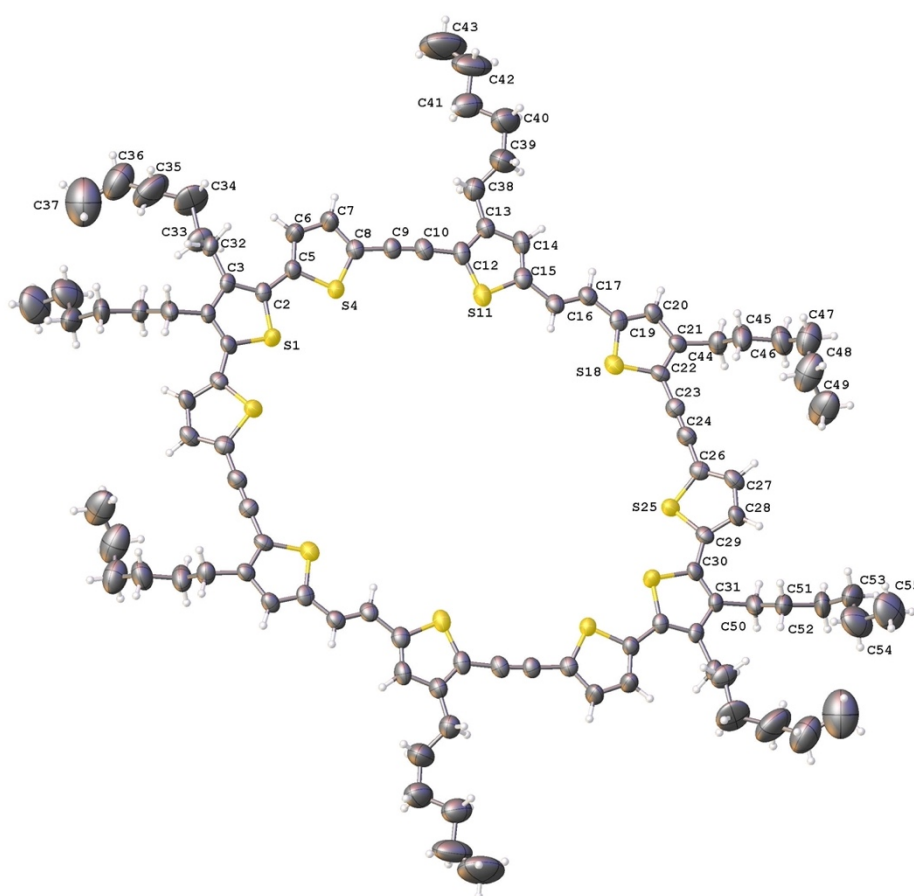
Figure S20. Selected molecular orbital density maps of **McT-2** (B3LYP/6311G d,p).



9. Crystallography

Single crystal x-ray diffraction data for **Mct1** were collected using Bruker D8 Venture equipped with Photon II CPAD detector, dual ImuS 3.0 Cu and Mo sources and n-Helix low temperature device. A red, plate-like crystal of dimensions 0.28 × 0.13 × 0.03 mm was selected, mounted in Fomblin perfluoropolyether oil and flash cooled to 150K. Selected crystallographic details are given below and full crystallographic data for CCDC 2063123 are available free of charge from the Cambridge Crystallographic Data Centre www.ccdc.cam.ac.uk.

Crystal data. $C_{100}H_{120}S_{10}$, $M = 1642.55$, triclinic, $a = 14.0049 (19)$, $b = 14.488 (2)$, $c = 14.624 (2)$ Å, $\alpha = 100.332 (6)^\circ$, $\beta = 115.884 (5)^\circ$, $\gamma = 109.458 (6)^\circ$, $U = 2325.3 (6)$ Å³, $T = 150$ K, space group $P-1$ (no.2), $Z = 1$, 17621 reflections measured, 9268 unique ($R^{\text{int}} = 0.090$), which were used in all calculations. The final $R[F^2 > 2\sigma(F^2)] = 0.113$ for 3477 reflections with $I > 2\sigma(I)$, $wR(F^2)$ was 0.33 (all data).



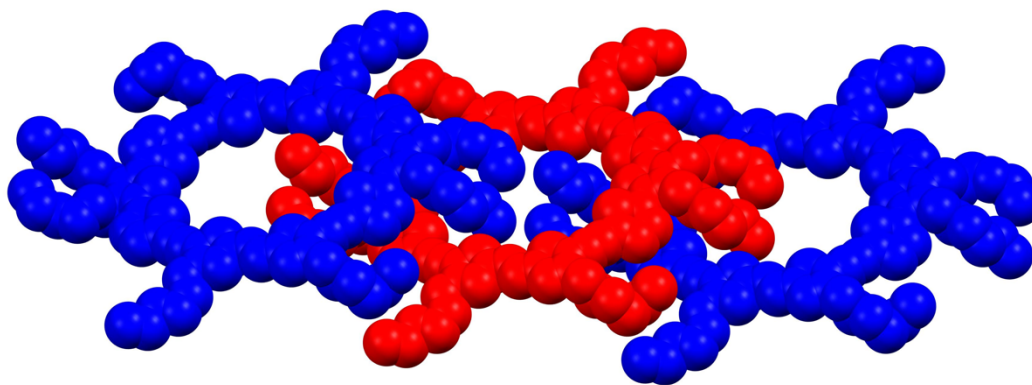


Figure S21. Above figure showing the structure and atom labelling scheme of **MCT-1**, atomic displacement ellipsoids drawn at 50% probability level and below showing the packing of MCT-1 showing the filling of the cavities by the alkyne chain from adjacent molecules.

10. Atomic Force Microscopy

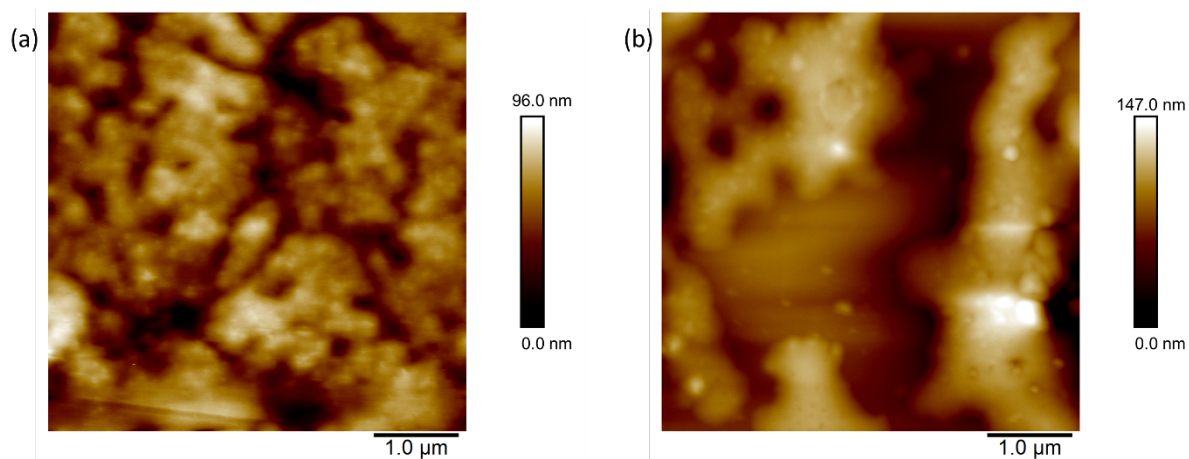


Figure S22. Tapping mode atomic force microscopy topography images for **MCT-1** films deposited from (a) chloroform (RMS roughness = 13.5 nm) and (b) toluene (RMS roughness = 23.7 nm). Scan area $5 \times 5 \mu\text{m}^2$

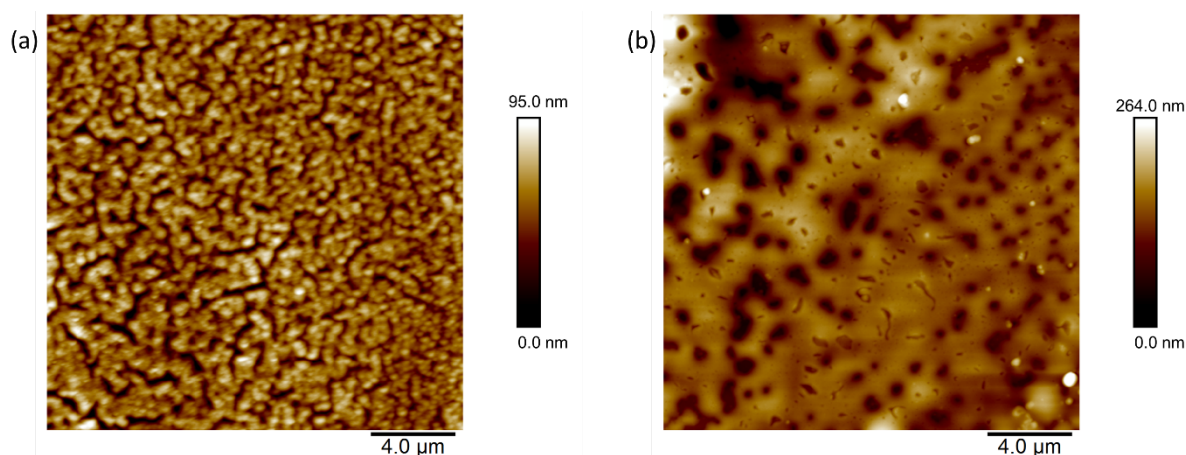


Figure S23. Tapping mode atomic force microscopy topography images for **MCT-1** films deposited from (a) chloroform (RMS roughness = 3.9 nm) and (b) toluene (RMS roughness = 12.8 nm). Scan area $20 \times 20 \mu\text{m}^2$

11. References

1. Gaussian 09, M. J. Frisch, G. W. Trucks, H. B. Schlegel, G. E. Scuseria, M. A. Robb, J. R. Cheeseman, G. Scalmani, V. Barone, G. A. Petersson, H. Nakatsuji, X. Li, M. Caricato, A. Marenich, J. Bloino, B. G. Janesko, R. Gomperts, B. Mennucci, H. P. Hratchian, J. V. Ortiz, A. F. Izmaylov, J. L. Sonnenberg, D. Williams-Young, F. Ding, F. Lipparini, F. Egidi, J. Goings, B. Peng, A. Petrone, T. Henderson, D. Ranasinghe, V. G. Zakrzewski, J. Gao, N. Rega, G. Zheng, W. Liang, M. Hada, M. Ehara, K. Toyota, R. Fukuda, J. Hasegawa, M. Ishida, T. Nakajima, Y. Honda, O. Kitao, H. Nakai, T. Vreven, K. Throssell, J. A. Montgomery, Jr., J. E. Peralta, F. Ogliaro, M. Bearpark, J. J. Heyd, E. Brothers, K. N. Kudin, V. N. Staroverov, T. Keith, R. Kobayashi, J. Normand, K. Raghavachari, A. Rendell, J. C. Burant, S. S. Iyengar, J. Tomasi, M. Cossi, J. M. Millam, M. Klene, C. Adamo, R. Cammi, J. W. Ochterski, R. L. Martin, K. Morokuma, O. Farkas, J. B. Foresman, and D. J. Fox, Gaussian, Inc., Wallingford CT, 2016.
2. Marques dos Santos, J. *et al.* Influence of alkyne spacers on the performance of thiophene-based donors in bulk-heterojunction organic photovoltaic cells. *Dye. Pigment.* **188**, 109152 (2021).
3. Roh, D. H. *et al.* Strategy for Improved Photoconversion Efficiency in Thin Photoelectrode Films by Controlling π -Spacer Dihedral Angle. *J. Phys. Chem. C* **120**, 24655–24666 (2016).